Heliyon 9 (2023) e13474

Contents lists available at ScienceDirect

Heliyon

journal homepage: www.cell.com/heliyon

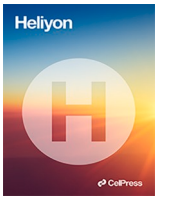

Research article

Investigation of the photoactivation effect of TiO_2 onto carbon-clay paste electrode by cyclic voltammetry analysis

Bakary Tigana Djonse Justin [a], Niraka Blaise [b], Hambate Gomdje Valery [b,*]

[a] Department of Chemistry, Faculty of Sciences, University of Maroua, P.O. Box 814, Maroua, Cameroon
[b] Department of Textile and Leather Engineering, National Advanced School of Engineering of Maroua, P.O. Box 46, Maroua, Cameroon

ARTICLE INFO

Keywords:
Cyclic voltammetry
Photoactivity
Ascorbic acid
Limit of detection
Limit of quantification

ABSTRACT

In this work, a cyclic voltammetry analysis for the detection of Ascorbic Acid (AA) based on a carbon-clay paste electrode modified with titanium dioxide (CPEA/TiO_2) is presented. The electrochemical sensor was prepared using clay and carbon graphite, mixed with TiO_2 to investigate the electrode behavior towards the detection of AA. Comprehensive characterization approaches including X-ray diffraction (XRD), Selected area electron diffraction (SAED), Transmission electron microscopy (TEM), Fourier transform infra-red spectroscopy (FTIR) were carried out on different samples. The results indicated that, the electrode has been effectively modified, while the electrochemical parameters of AA on CPEA/T_iO_2/UV such as the charge transfer coefficient (α_a), number of electrons (n) transferred and standard potential were calculated. CPEA/TiO_2/UV exhibit better photoactivity and also higher electronic conductivity under light radiation (100 W). The linear range for AA was determined between 0.150μM and 0.850 μM with the straight-line equation equivalent to $I_{pa}(\mu A) = 2.244[AA] + 1.234$ ($n = 8$, $R^2 = 0.993$). The limit of detection was 0.732 μM (3σ) and limit of quantification was 2.440 μM. For the analytical applications, pharmaceutical tablets such as Chloroquine phosphate, Azithromycin and Hydroxychloroquine sulfate were performed. In addition, interference study in the analytical application was performed, and it was found that the electroanalytical method used can be well adopted for simultaneous electrochemical detection of AA and Azithromycin.

1. Introduction

At present, modified electrodes constitute the most important alternative in electrochemistry because of the weight range of their applications since their surfaces are the place of oxidation-reduction reactions [1]. Modified electrodes are also used as electrochemical sensors according to their physico-chemical properties [2]. Carbon is widely used as a base material for the manufacture of conventional electrodes such as glassy carbon (GC), carbon nanotubes (CNT) or multiwall carbon nanotubes (MWCNT) [3–5]. It is well established as good electrical and thermal conductor with good chemical stability [6]. These reasons led to some researchers using carbon and their allotropic derivatives as basic materials to make sensors by modifying their surfaces to further increase their electrochemical detection capacity [7–9].

Clays materials are abundantly used in many industrial processes due to their physico-chemical properties such as specific surface area, cationic exchange capacity and d-spacing [10–12]. They are used as a catalytic support in adsorption phenomena [13–18] and in

* Corresponding author.
E-mail address: valeryhambate@gmail.com (H.G. Valery).

https://doi.org/10.1016/j.heliyon.2023.e13474
Received 18 August 2022; Received in revised form 26 January 2023; Accepted 31 January 2023
Available online 4 February 2023

electrochemistry to design sensors [19–21].

Several decades ago, Fujishima and Honda reported for the first time a research results on the hydrogen production on photo-electrodes made of titanium dioxide (T_iO_2) in ultraviolet light [22,23]. The photocatalysis with semi-conductors materials was considered as the most promising approach for both hydrogen production and pollution abatement. Today, TiO_2 is considered as a good photocatalytic support with regard to its narrow optical band gap energy estimated to 3.2eV for the anatase structure. Thus it allows its use in the photocatalysis and production of photoelectrochemical devices, as well as photovoltaics and sensors [24,25].

Recently, special attention has been focused on Chloroquine (CHL), Hydroxychloroquine (HCY) and Azithromycin (AZI) molecules due to the outbreak of the COVID-19 pandemic [26]. In fact, chloroquine and hydroxychloroquine are two chemical molecules of the same family generally used in the prevention of malaria and for their anti-inflammatory properties. They are also used for the treatment of several forms of lupus and rheumatoid arthritis [27]. On the other hand, Azithromycin is an azalide belonging to the macrolides family and has been used in the treatment of many bacterial infections [28]. As far as the Ascorbic Acid (AA) is concerned, it is well known as vitamin C present in fruits and has been well established as good antioxidant [29].

Several techniques employed for the detection of these molecules include: High Performance Liquid Chromatography (HPLC) [30,31], Gas Phase Chromatography (GPC) [32,33], simple spectrophotometric methods [34,35], capillary electrophoresis [36,37], flow injection analysis fluorescence [38] and calorimetry [39]. However, they have shown some limitations which include high prices, complexity of their implementation and the manipulation difficulty in-situ analyses compared to electroanalytic methods. Therefore, electroanalytic techniques have exhibited promising application due to their ease of implementation, high precision, inexpensiveness and easily transportable apparatus for in-situ analyses [40–43].

The present study aims to design an electrochemical sensor based on a carbon-clay paste electrode for which the preparation is carried out by a simplified method. The influence of the photoactivated TiO_2 in addition to the response provide by the electrochemical sensor in the detection of Ascorbic Acid (AA), Chloroquine phosphate (CHL), Hydroxycholoroquine sulfate (HYC) and Azithromycin (AZI) was investigated. In addition, this work contributes to the valorization of clay mineral from the far-north region of Cameroon which exhibit interesting physico-chemical properties.

2. Experimental

2.1. Chemical reagents

The Carbon graphite powder, Titanium dioxide, Ascorbic acid L (+) (99%), Ethanol and paraffin oil were purchased from Sigma Chemical Company. Potassium dihydrogen phosphate (KH_2PO_4) was purchased from Merck and the phosphate buffer solution (PBS) was prepared based on the compound. Choloroquine phosphate, Azithromycin and Hydroxychloroquine sulfate were used in pharmaceutical form. The natural clay material used in this work has been reported in previous work [44]. The clay sample was collected in the locality of Makabaye (Far North of Cameroon) with the following system coordinates: 10°34.393 N and 014°16.895 E. The fine fraction was obtained on the basis of Stockes law.

2.2. Analytical methods

Powder X-ray diffraction (XRD) measurements of the respective samples were performed using Bruker D8 Advance X-ray diffractometer equipped with a rotating anode of Cu Kα ($\lambda = 1.540$ A°) operated at 40 kV and 100 mA. Spectra were recorded in the 2θ range of 10°–50° at scan rate of 0.05°/min and the detection limit for a given crystalline phase is estimated at around 1% in mass. Joint Committee on Powder Diffraction Standards (JCDPS) XRD cards were used to provide essential information for the identification of clay minerals and modified clays. The transmission electron microscopy (Tecnai F20 (FEI) was used to observe the morphology of clays and modified clays samples at high resolution while data collection and tomography with important additional information was provided by the selected area electron diffraction at an acceleration voltage of 200 kV. It is equipped with a direct detector for improved spatial resolution at low sample dose conditions. The Fourier transform infrared spectroscopy (FT-IR) was recorded on a shimadzu 8400S FT-IR instrument using KBr in which pellet were homogenized by grinding a powder of KBr, hard-pressed using shimadzu MHP-1 hand press. The measurements were recorded in IR range of 400–4000 cm^{-1} with 45 scans. Electrochemical analysis was performed in cells equipped with three electrodes using a Pgstat-12 Autolabpotentiostat/galvanostat driven by general electrochemical systems for computer data processing (Volta Lab. master 4 software). A three-electrode system composed of carbon–clay paste electrode modified by TiO_2 which was use as the working electrode; a silver chloride electrode which was used as the reference electrode, while a platinum wire was used as the counter electrode. A device based on an electric lamp (100 W) was used as a source of light radiation.

2.3. Preparation of the working electrode

The carbon-clay paste electrode modified by TiO_2 was prepared by mixing 35% of carbon with 35% of clay and then 30% of titanium dioxide. The mixture was made using paraffin oil (7.2 mL) as a binder and ethanol as solvent. The paste was manually placed into the cylindrical cavity of the electrode (geometric surface of the working electrode is approximately 0.126 cm^2).

3. Results and discussion

3.1. X-ray diffraction analysis

The X-ray diffraction patterns of different samples show that clay is mainly constituted of phylosilicate minerals of type 2/1 (5.921°; 12.236°; 35.032°), low amounts of Quartz (26.627°) and Feldspath (27.901°). The peak having the d-spacing $d_{001} = 0.746$ nm is characteristic of hydrated Kaolinite disappeared when the clay is modified by carbon and then by TiO_2. This is due to the interfacial interactions between the functional groups present at the surface of the clay and the modifiers (carbon and TiO_2). The same phenomenon is observed with the peaks at 12.236° corresponding to d-spacing equal to 0.363 nm and characteristic of montmorillonite. The presence of an intense peak at 26.692° with d-spacing $d_{002} = 0.175$ nm is characteristic of carbon. It is also observed on the clay diffractogram but at low intensity, which might be due to the presence of organic materials in the samples [45]. The different respective peaks observed at 2θ equal to 36.093° and 41.231° are characteristic of titanium dioxide in the anatase form [46,47]. In general, these types of clays fix water (Cations, molecules, etc.) by adsorption on their surface and are called swelling clays. After drying, they develop a mechanical energy and this mechanical energy will decrease with the modification processes favoring interfacial interactions. Thus, the clay shrinks and the inter-foliar distances decreases (see Fig. 1).

3.2. Transmission electron microscopy and selected area electron diffraction

The surface microstructure of composite was analyzed using Transmission electron microscopy (TEM) and Selected area electron diffraction (SAED). The results are presented in Fig. 2. Fig. 2(a)–(c) exhibits the surface morphology of clays, carbon-clay and carbon-clay modified by titanium dioxide respectively. The surface morphology of different electrodes presents a superposition of sheets separated from each other by variable inter-reticular distance in the nanometric order. The carbon-clay paste electrode surface modification undergoes a change in morphology due to the formation of new bonds. The SAED image (Fig. 2(d)) displays overlapping diffraction patterns formed by concentric rings with illuminated area composed of several crystallites of different orientation in an excellent agreement with XRD results. This image is typical of polycrystalline samples such as clays. The inter-reticular distances as calculated from the peak diffraction are in agreement with this image and confirm that the materials studied are polycrystalline [48].

3.3. Fourier transform infrared spectroscopy analysis

The functionals groups on the surface of different electrodes were analyzed and presented in Fig. 3. The –OH vibrations and Si–O absorption bands occurred at 3701 and 513 cm^{-1} respectively. These absorption bands are important in differentiating clay minerals [49]. The spectrum of the clay (Fig. 3(a)) contains a band at 513 cm^{-1}, characteristic of the vibrations of the absorption bands of the Si–O–Al bonds present in the phylosilicate clays of the 2/1 types. This predicts the presence of Kaolinites in the clay material. After modification of the clay by carbon and TiO_2, there is the appearance of a band at 998 cm^{-1} which is characteristic of the vibrations of the absorption bands of the Si–O–Ti bonds implying that there has been cation exchange and, the intensity of this band increase with the substitution of alumina by titanium. Also, peaks of absorption bands are found between 1632 and 1640 cm^{-1}, are characteristic of C=C bond in different materials. The presence of these peaks in the clay material is explained by the presence of organic residues before the treatment. After modification by carbon, the peak increases in density, this shows that the material is indeed modified by

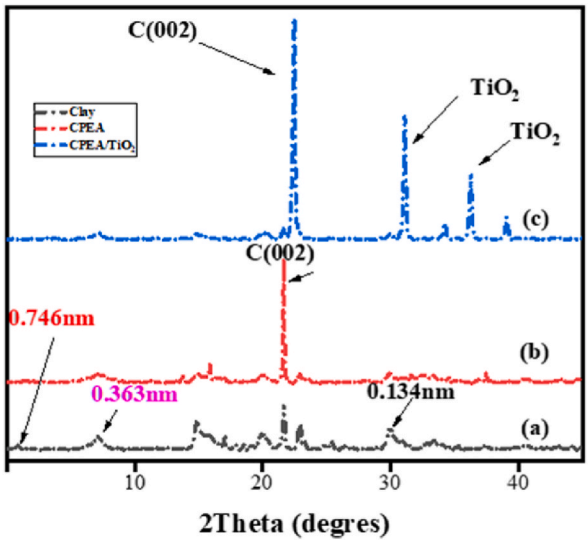

Fig. 1. XRD patterns of different electrodes: (a) Clay, (b) CPEA, (c) CPEA/TiO2.

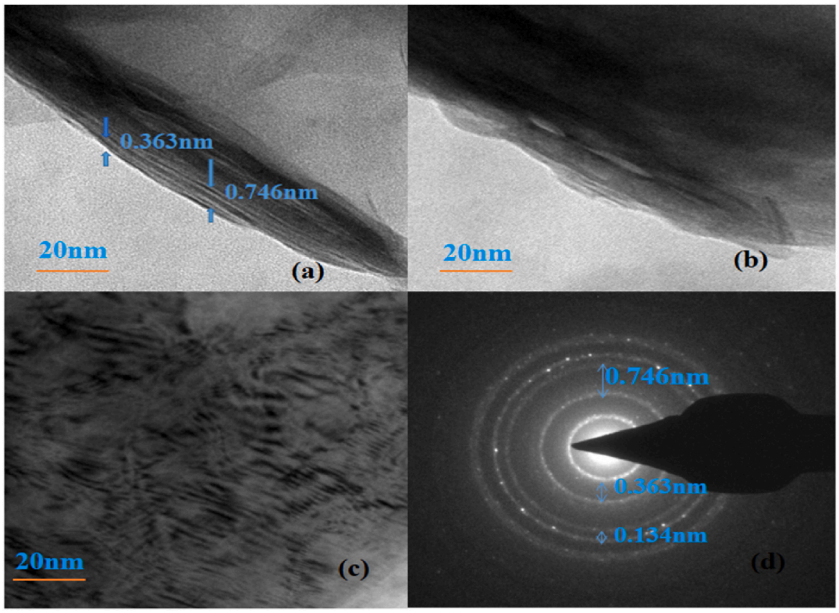

Fig. 2. TEM images of (a) Clay sheets, (b) CPEA, (c) CPEA/TiO2, (d) SAED pattern of clay.

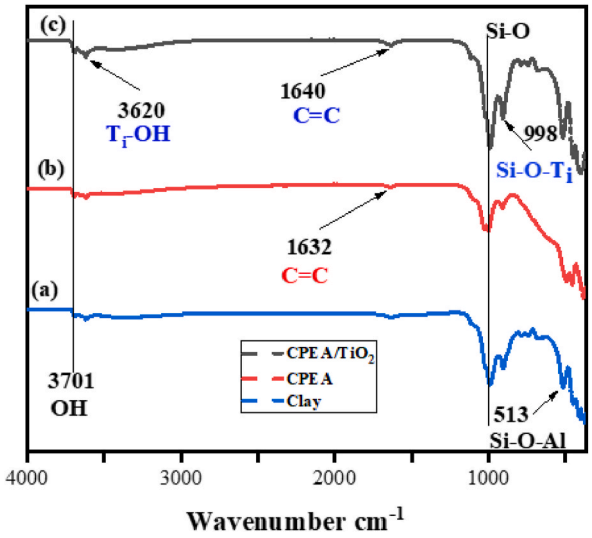

Fig. 3. Infra-Red spectra:(a) Clay, (b) CPEA, (c) CPEA/TiO2. (For interpretation of the references to colour in this figure legend, the reader is referred to the Web version of this article.)

carbon. These results show that there are interfacial interactions during the modification process of the clay. Between 3620 and 3701 cm^{-1}, the vibrations of the OH absorption bands are perceptible, more specifically at 3620 cm^{-1}, this vibration is characteristic of Ti–OH bonds [50].

3.4. Electrochemical investigation

3.4.1. Electrochemical behavior of AA onto carbon-clay paste electrode modified by TiO_2

The behavior of the carbon-clay modified by TiO_2 under a radiation light is illustrated in Fig. 5. The cyclic voltammograms were recorded at a scan rate of 50 mV/s in a 0.1 M phosphate buffer solution and pH = 6.4 containing 0.30 μM of AA. An AA oxidation peak is observed at 0.121 V corresponding to an anode current density of 18.20×10^{-6} $A.cm^{-2}$ for the carbon-clay paste electrode (CV CPEA) which show a low charge transfer. With the carbon-clay paste electrode modified by TiO_2 not subjected to light radiation, there is a displacement of the anode potential at 0.148 V corresponding to an oxidation current density of 24.520×10^{-6} A cm^{-2} and this

value increases slightly reflecting a charge transfer due to the presence of TiO_2. When the carbon-clay paste electrode is modified by TiO_2 and subjected to light radiation, the oxidation current density increases intensely to a value of 50.120×10^{-6} A cm^{-2} with a displacement potential of 0.171 V. AA molecules in the solution are adsorbed on the surface of CPEA/TiO_2/UV and then oxidized in close agreement with the literature [51]. The oxidation process of AA releases electrons and the photocurrent density is detected at a constant working voltage. The photocurrent density increases twice when the TiO_2 is photoactivated. This reflects a significant transfer of charges which is explained by the semi-conductor behavior of TiO_2 which is known by its ability to react after having absorbed a light source of wave length lower than its band gap [52]. The photocatalytic activity of TiO_2 depends on the intensity of the absorption light. Better photocatalytic efficiency can be achieved with an increase in the intensity of light as it improves charge separation. Photoactivation of TiO_2 by light radiation allows the production of electrons (e)/hole (h^+) pairs when they absorb a photon with energy equals to their band gap or higher than that [53]. The mechanism is illustrated in Fig. 4.

The holes formed in the valence band will migrate to the surface of the electrode and may be involved in the surface oxidation reaction of CPEA/TiO_2/UV, which probably justifies the increase in current density with generation of a photocurrent. This phenomenon is well known as photocatalysis [53].

3.4.2. Enhanced electrochemistry behavior of CPEA/TiO_2/UVtoward AA detection

Fig. 6 shows the electrochemical behavior of ascorbic acid (AA) at the carbon-clay paste modified by TiO_2 (CPEA/TiO_2/UV) under light radiation using a 100 W lamp in a 0.1 M phosphate buffer electrolyte solution and pH = 6.4 at a scan rate of 50 mV/s compared to carbon-clay paste electrode (CPEA) and carbon-clay paste electrodes modified by TiO_2 is not subjected to light radiation (CPEA/TiO_2). At the potential ranging from −0.2 V to 0.7 V, in the presence of 0.30 μM of (AA), an intense peak which appears at 0.181 V (CV (b)) in the direction of the anodic scan, reflecting an oxidation reaction of AA. This reaction is rapid and irreversible, showing a rapid phenomenon of charge transfer to the surface of the electrode, which is probably due to T_iO_2, known for its semi-conductor capacity [52]. For the cyclic voltammogram (a) recorded by the carbon-clay paste electrode (CPEA) in a 0.1 M phosphate buffer electrolyte solution and pH = 6.4 at a scan rate of 50 mV/s in the absence of AA, no peak is observed on the cyclic voltammogram which suggests that at the chosen potential range interval no electroactive species is present on the surface of the CPEA.

3.4.3. Effect of potential scan rate

The scan rate effect is illustrated in Fig. 7(a). It shows that the peaks of the oxidation current densities increase with scan rate (v). The related regression line (Fig. 7(b)) with $I_{Pa} = f(v^{1/2})$ makes it possible to obtain straight-line equation:

$$I_{Pa} \times \left(10^{-6}\right) = 54.020[v]^{1/2} + 4.774$$

with the regression coefficient $R^2 = 0.976$.

This suggests that the electrochemical reaction process at CPEA/TiO_2/UV is controlled by the diffusion phenomenon.

The electrochemical mechanism which takes place on the surface of CPEA/T_iO_2/UV can be confirmed by the determination of the charge transfer coefficient (α_a) and the number of electrons (n) transferred. Fig. 8(a) exhibits the oxidation peak current density (E_{pa}) as a function of scan rate. The coordinates at the origin of the line $E_{pa} = f(v)$ makes it possible to obtain the value of the standard potential E_0 at 0.128 V. The equation of the straight-line $E_{pa} = f(v)$ is:

$$E_{pa} = 0.087v + 0.128$$

with the regression coefficient R2 = 0.991.

Fig. 8(b) gives the straight-line $\ln I_{pa} = f(E_{pa} - E_0)$ with equation:

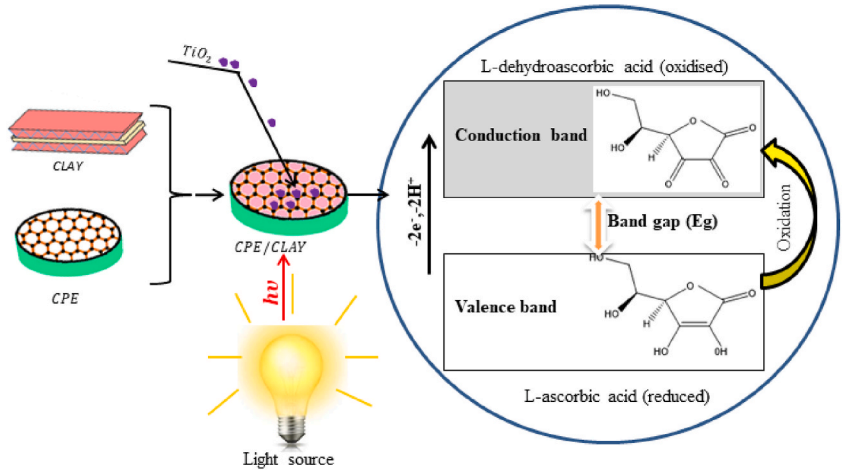

Fig. 4. Illustration of the mechanism of degradation by light radiation of the oxidation of Ascorbic Acid at the CPEA/TiO2/UV electrode.

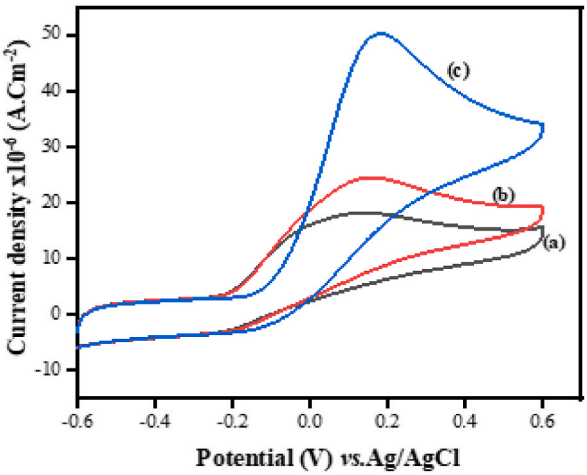

Fig. 5. Cyclic Voltammograms of (a) 0.30 μM of AA on CPEA, (b) 0.30 μM of AA on CPEA/TiO2, (c) 0.30 μM of AA on CPEA/TiO2/UV in 0.1 M PBS solution and pH = 6.4 at a scan rate of 50 mV/s.

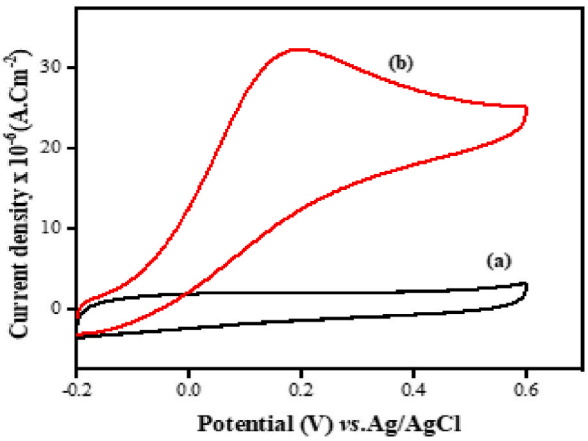

Fig. 6. Cyclic voltammograms of (a) in absence of AA on CPEA, (b) in presence of 0.30 μM of AA on CPEA/TiO2/UV in 0.1 M PBS solution and pH = 6.4 at a scan rate of 50 mV/s.

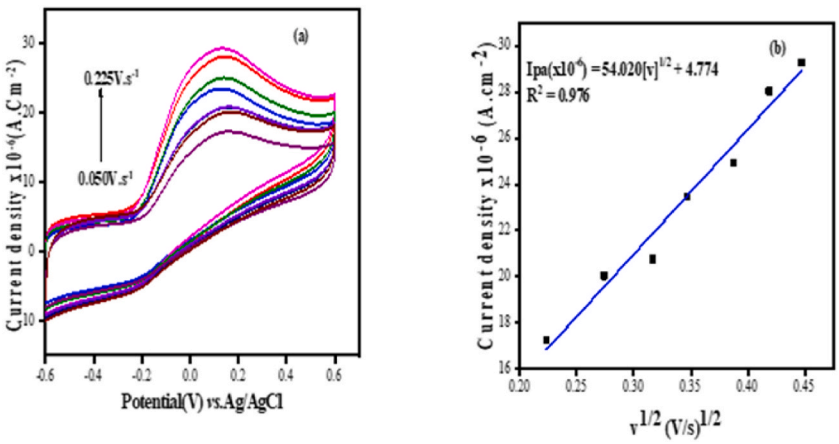

Fig. 7. (a) Cyclic voltammograms of AA at CPEA/TiO2/UV in 0.1 M PBS solution and pH = 6.4 at different scan rates (0.050–0.225 V s^{-1}, (b) calibration plots for the oxidation peak currents vs the square root of scan rate.

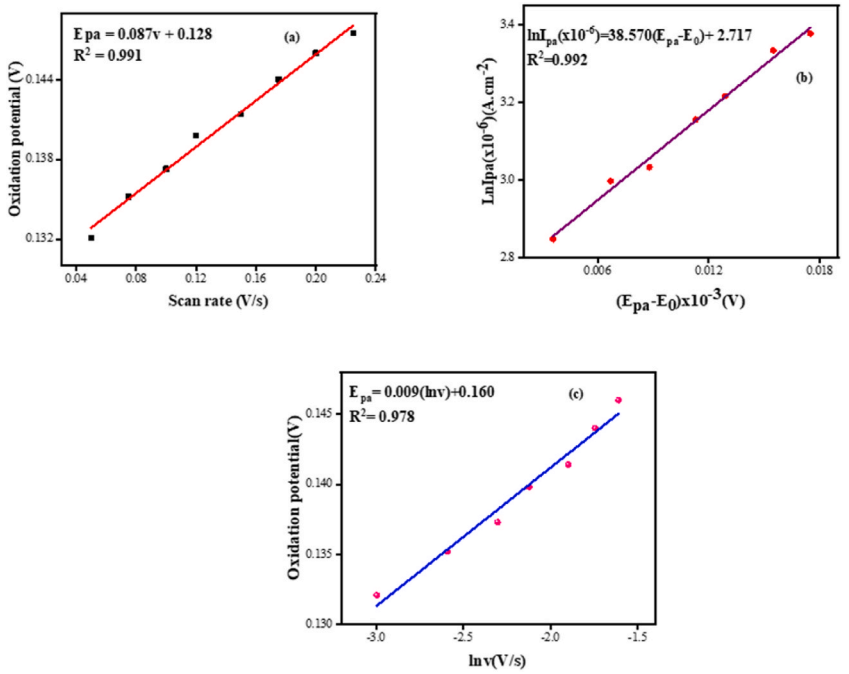

Fig. 8. (a) Experimental variation of oxidation potential as a function of scan rate (b) experimental variation of peak current (ln Ipa) as a function of the difference of $E_{pa}-E_0$; (c) experimental variation of peak current (lnv) against a function of E_{pa}.

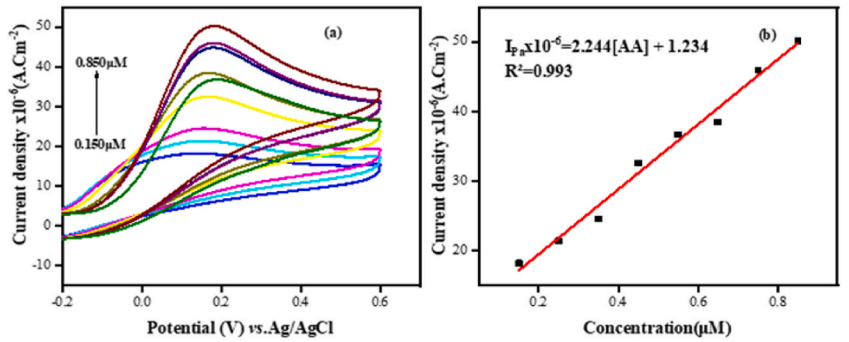

Fig. 9. (a) Cyclic voltammograms of AA at CPEA/TiO2/UV in 0.1 M PBS solution and pH = 6.4 at range of concentration [0.150 μM–0.850 μM] at a scan rates 50 mV/s, (b) calibration plots for the oxidation peak currents vs concentration.

$$\ln I_{pa} \times 10^{-6} = 38.570\left(E_{pa} - E_0\right) + 2.717$$

with the regression coefficient of 0.992.

The charge transfer coefficient during the oxidation process is given by Eq. (1) below:

$$\alpha_a = \frac{RTd \ln I_{pa}}{nFdE} \tag{1}$$

R, F and T are thermodynamic parameters used in working conditions, ideal gas constant, Faraday constant and absolute temperature.

The value of the charge transfer coefficient is obtained from Fig. 8(c) and the slope of the equation of the line lnv*vs*E_{Pa}:

$$E_{pa} = 0.009 \ln v + 0.160$$

with the regression coefficient $R^2 = 0.978$.

The calculations led to the determination of $\alpha_a = 0.224$ and by substituting in Eq. (2) with the number of electrons exchanged during the oxidation process of AA equal to 1.899 (≈2).

$$m = \frac{RT}{(1-\alpha_a)nF} \quad (2)$$

3.4.4. Effect of ascorbic concentration

The effect of AA concentration was studied in a 0.1 M phosphate buffer solution in the concentration range of 0.150 μM–0.850 μM. Using cyclic voltammetry to assess the sensitivity of CPEA/T_iO_2/UV, the current densities of AA oxidation peaks increase with concentration according to straight-line equation:

$$I_{pa} \times 10^{-6} = 2.244[AA] + 1.234$$

and a regression coefficient $R^2 = 0.993$.

The limits of detection and quantification are respectively equal to 0.732 μM and 2.440 μM. The limit of detection (LOD) calculated in the present work is compared to those reported in the literature and presented in Table 1.

3.5. Analytical application

3.5.1. Electro-oxidation of chloroquine phosphate, hydroxychloquine sulfate and azithromycin onto CPEA/T_iO_2/UV

The electrochemical behavior of the CPEA/T_iO_2/UV was studied by testing with tablets such as chloroquine phosphate (CHL), hydroxychloroquine sulfate (HYC) and azithromycin (AZI) in a 0.1 M PBS solution (pH = 6.4) at a scan rate of 50 mV/s (see Fig. 9). Fig. 10 shows the cyclic voltammograms of the different tablets with CPEA/T_iO_2/UV electrode. In the potential range [−0.1 V, 0.9 V], and the various tablets having the same concentrations (4 mM), there is appearance of an intense peak at 0.533 V corresponding to the oxidation potential of alcohol function in the molecule of AZI. The density of the peak of the current decreases significantly during the degradation of the CHL (E = 0.535 V) which implies there is displacement of the potential due to the environment of the degraded function and takes place slowly with regard to the photocurrent density of oxidation. The degradation of HYC takes place at a potential of 0.520 V corresponding to the oxidation potential of alcohol function. The alcohol function is oxidized but the current density is low which is justified by a low charge transfer during the degradation of the CHL molecule. The increase of the photocurrent generated during the degradation of AZI is due to the mobility of the species involved during the degradation. This mobility can result from the combination of initial Ti^{3+} and the Ti^{3+} generated by the light source. In the presence of HYC and CHL, the difference in the photocurrent generated is not considerable. It proves that the initial Ti^{3+} does not manage to cross the band gap and this also reveals the role of the state of surface in the trapping of the mobile Ti^{3+} thus decreasing the photocurrent [59]. These results show that the CPEA/TiO_2/UV electrode exhibits a more pronounced electrochemical response for the AZI molecule compared to the others.

3.5.2. Electrochemical behavior of a mixture of AA and AZI at CPEA/TiO_2/UV

The oxidation of 0.30 μM of AA and 0.150 μM of Azithromycin with CPEA/TiO_2/UV is shown. Fig. 11 shows a cyclic voltammogram with two oxidation potentials at 0.102 V which correspond to the degradation of Azithromycin, while the peak of AA oxidation appears at 0.210 V. This shows that the CPE/TiO_2/UV electrode gives a better response to Azithromycin than to AA, even though the concentration of AA was about 2 times higher than that of AZI.

In addition, the current density was found to be different which can be due to the difference in concentration, however, it seems less plausible. In fact, TiO_2 has a photocatalytic effect during the oxidation of Azithromycin because the oxidation potential appears before that of AA and during the oxidation of AZI the photocurrent generated crosses the band gap more quickly. The CPEA/TiO_2/UV electrode is more sensitive to the detection of Azithromycin.

4. Conclusion

In this study, it was demonstrated that the prepared CPEA/TiO_2/UV presented satisfactory sensitivity, selectivity and stability in sensing the AA in 0.1 M PBS at pH = 6.4. The modified electrode prepared was characterized by X-ray diffraction (XRD), Transmission electron microscopy (TEM), Selected area electron diffraction (SAED), and Fourier Transform infra-red (FT-IR). The analyses have shown that the electrode is indeed modified and exhibits physico-chemical properties capable of interacting with other molecules in solution. The carbon-clay paste electrode modified by T_iO_2 has a high sensitivity due to the increase in current density during photoactivation. A photocurrent is produced. The electrochemical behavior of the AA molecule was studied and it appears that the

Table 1
Comparison of the performance of some electrodes with other analytical methods for Ascorbic Acid.

Electrodematerial	Technique used	Linear range	Limit of Detection AA	Reference
Ti–C-Tx/GCE	CV	100–1000 μM	0.075 μM	[41]
MWCNT-AONPSPCE	SWV	0.160–0.640 μM	140 nM	[54]
PVP-GR/GCE	LSV	4 μM–1 mM	0.80 μM	[55]
Fe_3O_4NPsSPCE	SWV	10–100 μM	15.7 μM	[56]
Sonigel-carbone ME	SWV	50–1000 μM	50 μM	[57]
RGO-ZnO/GCE	DPV	50–235 μM	3.71 μM	[58]
CPEA/TiO_2/UV	CV	0.150–0.850 μM	0 .732 μM	Present work

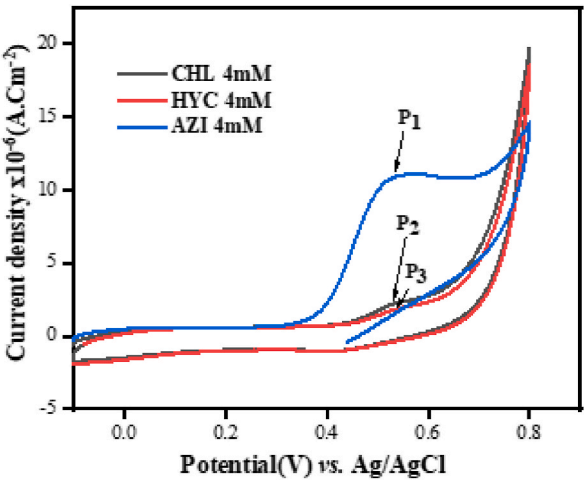

Fig. 10. Cyclic voltammograms of 4 mM of Chloroquine phosphate (CHL), 4 mM Hydroxychloquine sulfate (HYC) and 4 mM azithromycin on CPEA/TiO2/UV in 0.1 M PBS solution and pH = 6.4 at a scan rate of 50 mV/s.

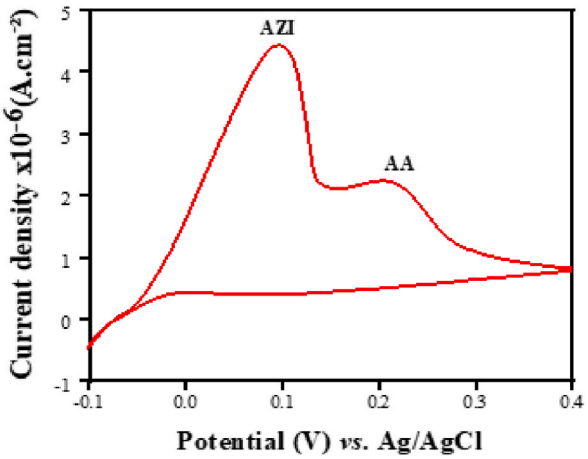

Fig. 11. Cylic voltammograms for a mixture of 0.30 μM Ascorbic Acid (AA) and 0.150 μM Azithromycin in 0.1 M PBS solution and pH = 6.4 at a scan rate of 50 mV/s at CPEA/TiO2/UV.

prepared sensor has a good electrochemical response to the AA molecule. A Limit of detection of the order of 0.732 μM was obtained. The carbon-clay paste electrode modified by T_iO_2 shows interesting findingfor simultaneous detection of AA and AZI. The electrochemical sensor was also effectively employed for the detection of some tablets as choloroquine phosphate, hydroxychloroquine sulfate and azithromycin. Due to its sensitivity and repeatability of CPEA/TiO_2/UV, it has high potential for the future developments of electrochemical sensor and environmental research.

Author contribution statement

Bakary Tigana Djonse Justin: Performed the experiments; Analyzed and interpreted the data; Wrote the paper.

Niraka Blaise, Hambate Gomdje Valery: Conceived and designed the experiments; Analyzed and interpreted the data; Contributed reagents, materials, analysis tools or data.

Funding statement

This research did not receive any specific grant from funding agencies in the public, commercial, or not for profit sectors.

Data availability statement

Data will be made available on request.

Additional information

No additional information is available for this paper.

Declaration of interest's statement

The authors declare that they have no known competing financial interests or personal relationships that could have appeared to influence the work reported in this paper.

References

[1] B. Anerise, F. Mariselma, C. Constantino, B. José, F. Marystela, Synergy between polyaniline and OMt clay mineral in Langmuir-Blodgett films for the simultaneous detection of traces of metal ions, ACS Appl. Mater. Interfaces 7 (12) (2015), https://doi.org/10.1021/acsami.5b00187.

[2] N. Zhang, F. Qu, H.Q. Luo, N.B. Li, Sensitive and selective detection of biothiols based on target-induced agglomeration of silver nanoclusters, Biosens. Bioelectron. 42 (2013) 214–218, https://doi.org/10.1016/j.bios.2012.10.090.

[3] J. Wang, Ü. AnikKirgöz, J.-W. Mo, J. Lu, A. Nasser Kawde, A. Muck, Glassy carbon pasteelectrodes, Electrochem. Commun. 3 (4) (2001) 203–208, https://doi.org/10.1016/S1388-2481(01)00142-4.

[4] G. Jashari, I. Švancara, M. Sýs, Characterisation of carbon paste electrodes bulk-modified with surfactants for measurements in nonaqueous media, Electrochim. Acta 410 (2022), 140047, https://doi.org/10.1016/j.electacta.2022.140047.

[5] P.V. Narayana, T. MadhusudanaReddy, P. Gopal, M. Mohan Reddy, G. Ramakrishna Naidu, Electrocatalytic boost up of epinephrine and its simultaneous resolution in the presence of serotonin and folic acid at poly(serine)/multi-walled carbon nanotubes composite modified electrode: a voltammetric study, Mater. Sci. Eng. C 56 (2015) 57–65, https://doi.org/10.1016/j.msec.2015.06.011.

[6] B.A. Newcomb, Processing, structure, and properties of carbon fibers, Compos. Appl. Sci. Manuf. 91 (2016) 262–282, https://doi.org/10.1016/j.compositesa.2016.10.018.

[7] H. Shaoying, H. Ping, X. Zhang, Z. Xiaojuan, K. Liu, L. Jia, F. Dong, Poly(glycine)/graphene oxide modified glassy carbon electrode: preparation, characterization and simultaneous electrochemical determination of dopamine, uric acid, guanine and adenine, Anal. Chim. Acta (2018), https://doi.org/10.1016/j.aca.2018.06.020.

[8] Y. Li, Z. Ye, J. Zhou, J. Liu, G. Song, K. Zhang, B. Ye, A new voltammetric sensor based on poly(L-arginine)/graphene–Nafion composite film modified electrode for sensitive determination of Terbutaline sulfate, J. Electroanal. Chem. 687 (2012) 51–57, https://doi.org/10.1016/j.jelechem.2012.09.045.

[9] A.K. Bhakta, R.J. Mascarenhas, O.J. D'Souza, A.K. Satpati, S. Detriche, Z. Mekhalif, J. Dalhalle, Iron nanoparticles decorated multi-wall carbon nanotubes modified carbon paste electrode as an electrochemical sensor for the simultaneous determination of uric acid in the presence of ascorbic acid, dopamine and L-tyrosine, Mater. Sci. Eng. C Mater. Biol. Appl. 57 (2015) 328–337, https://doi.org/10.1016/j.msec.2015.08.003.

[10] R. Pusch, Chapter 6 mechanical properties of clays and clay minerals, vol. 1, in: F. Bergaya, B.K.G. Theng, G. Lagaly (Eds.), Developments in Clay Science, Elsevier, 2006, pp. 247–260, https://doi.org/10.1016/S1572-4352(05)01006-8.

[11] T.T. Zhu, C.H. Zhou, F.B. Kabwe, Q.Q. Wu, C.S. Li, J.R. Zhang, Exfoliation of montmorillonite and related properties of clay/polymer nanocomposites, Appl. Clay Sci. 169 (2019) 48–66, https://doi.org/10.1016/j.clay.2018.12.006.

[12] C. Tournassat, I.C. Bourg, C.I. Steefel, F. Bergaya, Chapter 1 – surface properties of clay minerals, vol. 6,, in: C. Tournassat, C.I. Steefel, I.C. Bourg, F. Bergaya (Eds.), Developments in Clay Science, Elsevier, 2015, pp. 5–31, https://doi.org/10.1016/B978-0-08-100027-4.00001-2.

[13] A. Awasthi, P. Jadhao, K. Kumari, Clay nano-adsorbent: structures, applications and mechanism for water treatment, SN Appl. Sci. 1 (9) (2019) 1076, https://doi.org/10.1007/s42452-019-0858-9.

[14] T. Zhang, W. Wang, Y. Zhao, H. Bai, T. Wen, S. Kang, G. Song, S. Song, S. Komarneni, Removal of heavy metals and dyes by clay-based adsorbents: from natural clays to 1D and 2D nano-composites, Chem. Eng. J. 420 (2021), 127574, https://doi.org/10.1016/j.cej.2020.127574.

[15] P. Liu, L. Zhang, Adsorption of dyes from aqueous solutions or suspensions with clay nano-adsorbents, Separ. Purif. Technol. 58 (1) (2007) 32–39, https://doi.org/10.1016/j.seppur.2007.07.007.

[16] S.C.R. Santos, Á.F.M. Oliveira, R.A.R. Boaventura, Bentonitic clay as adsorbent for the decolourisation of dyehouse effluents, J. Clean. Prod. 126 (2016) 667–676, https://doi.org/10.1016/j.jclepro.2016.03.092.

[17] S. Gu, X. Kang, L. Wang, E. Lichtfouse, C. Wang, Clay mineral adsorbents for heavy metal removal from wastewater: a review, Environ. Chem. Lett. 17 (2) (2019) 629–654, https://doi.org/10.1007/s10311-018-0813-9.

[18] M. Shahadat Momina, S. Isamil, Regeneration performance of clay-based adsorbents for the removal of industrial dyes: a review, RSC Adv. 8 (43) (2018) 24571–24587, https://doi.org/10.1039/C8RA04290J.

[19] B. Niraka, V.G. Hambate, M. Raja, O. Mohamed, J.T.D. Bakary, E.A. Ofudje, C. Abdelilah, Simultaneous electrochemical detection of Pb and Cd by carbon paste electrodes modified by activated clay, J. Anal. Methods Chem. 2022 (2022) e6900839, https://doi.org/10.1155/2022/6900839.

[20] Y. Gómez, L. Fernández, C. Borrás, J. Mostany, B. Scharifker, Characterization of a carbon paste electrode modified with tripolyphosphate-modified kaolinite clay for the detection of lead, Talanta 85 (3) (2011) 1357–1363, https://doi.org/10.1016/j.talanta.2011.06.014.

[21] T.V. Sathisha, B.E.K. Swamy, S. Reddy, B.N. Chandrashekar, B. Eswarappa, Clay modified carbon paste electrode for the voltammetricdetection of dopamine in presence of ascorbic acid, J. Mol. Liq. 172 (2012) 53–58.

[22] A. Fujishima, K. Honda, Electrochemical photolysis of water at a semiconductor electrode, Nature 238 (5358) (1972) 37–38, https://doi.org/10.1038/238037a0.

[23] L.-L. Long, A.-Y. Zhang, J. Yang, X. Zhang, H.-Q. Yu, A green approach for preparing doped TiO_2 single crystals, ACS Appl. Mater. Interfaces 6 (19) (2014) 16712–16720, https://doi.org/10.1021/am503661w.

[24] S. Aftab, N.K. Bakirhan, O. Esim, A. Shah, A. Savaser, Y. Ozkan, S.A. Ozkan, NH_2-fMWCNT-titanium dioxide nanocomposite based electrochemical sensor for the voltammetric assay of antibiotic drug nadifloxacin and its in vitro permeation study, J. Electroanal. Chem. 859 (2020), 113857, https://doi.org/10.1016/j.jelechem.2020.113857.

[25] B. Gao, Z. Liang, D. Han, F. Han, W. Fu, W. Wang, Z. Liu, L. Niu, Molecular lyimprinted photo-electrochemical sensor for hemoglobin detection based on titaniumdioxide nanotube arrays loaded with CdS quantum dots, Talanta 224 (2021), 121924, https://doi.org/10.1016/j.talanta.2020.121924.

[26] H. Mater Mahnashi, A.M. Mahmoud, A. Saad Alkahtani, M.M. El-Wekil, Simultaneous electrochemical detection of azithromycin and hydroxychloroquine based on VS_2 QDs embedded N, S @graphene aerogel/cCNTs 3D nanostructure, Microchem. J. 163 (2021), 105925, https://doi.org/10.1016/j.microc.2021.105925.

[27] X. Peng, Activation of peroxy monosulfate by single atom Co-N-C catalysts for high-efficient removal of chloroquine phosphate via non-radical pathways: electron-transfer mechanism, Chem. Eng. J. (2021), 132245-132245.

[28] O. Vajdle, V. Guzsvány, D. Škori, J. Csanádi, M. Petkovi, M. Avramov-Ivi, Z. Kónya, S. Petrovi, A. Bobrowski, Voltammetric behavior and determination of the macrolide antibiotics azithromycin, clarithromycin and roxithromycin at a renewable silver – amalgam film electrode, Electrochim. Acta 229 (2017) 334–344, https://doi.org/10.1016/j.electacta.2017.01.146.

[29] M.A. Green, S.C. Fry, Vitamin C degradation in plant cells via enzymatic hydrolysis of 4-O-oxalyl-L-threonate, Nature 433 (7021) (2005) 83–87, https://doi.org/10.1038/nature03172.

[30] K.K. Chebrolu, G.K. Jayaprakasha, K.S. Yoo, J.L. Jifon, B.S. Patil, An improved sample preparation method for quantification of ascorbic acid and dehydroascorbic acid by HPLC, LWT – Food Sci. Technol. 2 (47) (2012) 443–449, https://doi.org/10.1016/j.lwt.2012.02.004.

[31] A.H.H. Bakheit, B.M.H. Al-Hadiya, A.A. Abd-Elgalil, Chapter one - azithromycin, in: H.G. Brittain (Ed.), Profiles of Drug Substances, Excipients and Related Methodology 39, Academic Press, 2014, pp. 1–40, https://doi.org/10.1016/B978-0-12-800173-8.00001-5.

[32] F.O. Silva, Total ascorbic acid determination in fresh squeezed orange juice by gas chromatography, Food Control 16 (1) (2005) 55–58, https://doi.org/10.1016/j.foodcont.2003.11.007.

[33] S. Bodur, S. Erarpat, Ö.T. Günkara, S. Bakırdere, Accurate and sensitive determination of hydroxychloroquine sulfate used on COVID-19 patients in human urine, serum and saliva samples by GC-MS, J. Pharm. Anal. 11 (3) (2021) 278–283, https://doi.org/10.1016/j.jpha.2021.01.006.

[34] I.S.A. Porto, J.H. Santos Neto, L.O. dos Santos, A.A. Gomes, S.L.C. Ferreira, Determination of ascorbic acid in natural fruit juices using digital image colorimetry, Microchem. J. 149 (2019), 104031, https://doi.org/10.1016/j.microc.2019.104031.

[35] D. Bhadra, S. Bhadra, N.K. Jain, PEGylated peptide dendrimeric carriers for the delivery of antimalarial drug chloroquine phosphate, Pharm. Res. 23 (3) (2006) 623–633, https://doi.org/10.1007/s11095-005-9396-9.

[36] B.M.C. Costa, A.A. Prado, C.O. Thiago, L.P. Bressan, R.A.A. Munoz, A.D. Batista, J.A.F. da Silva, E.M. Richter, Fast methods for simultaneous determination of arginine, ascorbic acid and aspartic acid by capillaryelectrophoresis, Talanta 204 (2019) 353–358, https://doi.org/10.1016/j.talanta.2019.06.017.

[37] X. Sun, W. Ding, C. Chen, T. Yu, Q. Chen, K.W. Ding Yang, Evaluation of poly(glycidylmethacrylate)-coated column for enantioseparation with azithromycin lactobionate and clindamycin phosphate as chiral selectors in capillary electrophoresis, Chromatographia 84 (5) (2021) 499–505, https://doi.org/10.1007/s10337-021-04029-8.

[38] A. Moreno-Cid, M.C. Yebra, X. Santos, Flow injection determinations of citric acid: a review, Talanta 63 (3) (2004) 509–514, https://doi.org/10.1016/j.talanta.2003.12.009.

[39] C. Garnero, M. Longhi, Study of ascorbic acid interaction with hydroxypropyl-beta-cyclodextrin and triethanolamine, separately and in combination, J. Pharm. Biomed. Anal. 45 (4) (2007) 536–545, https://doi.org/10.1016/j.jpba.2007.07.030.

[40] G. Veerapandi, S. Meenakshi, S. Anitta, C. Arul, P. Ashokkumar, C. Sekar, Precise and quick detection of ascorbic acid and eugenol in fruits, pharmaceuticals and medicinal herbs using hydroxyapatite-titaniumdioxide nanocomposite-based electrode, Food Chem. (2022), 132251-132251,.

[41] N. Murugan, R. Jerome, M. Preethika, A. Sundaramurthy, A.K. Sundramoorthy, 2D-titanium carbide (MXene) based selective electrochemical sensor for simultaneous detection of ascorbic acid, dopamine and uric acid, J. Mater. Sci. Technol. 72 (2021) 122, https://doi.org/10.1016/j.jmst.2020.07.037.

[42] J. López-Flores, M.L. Fernández-De Córdova, A. Molina-Díaz, Multicommutated flow-through optosensor simplemented with photochemically induced fluorescence: determination of flufenamic acid, Anal. Biochem. 361 (2) (2007) 280–286, https://doi.org/10.1016/j.ab.2006.11.020.

[43] I. Kenfack, E. Ngameni, F.M. TchienoMelataguia, A. Walcarius, Organoclay-modified electrodes: preparation, characterization and recent electroanalytical applications, J. Solid State Electrochem. 19 (2015), https://doi.org/10.1007/s10008-014-2728-0.

[44] D. Rallet, A. Paltahe, C. Tsamo, B. Loura, Synthesis of clay-biochar composite for glyphosate removal from aqueous solution, Heliyon 8 (3) (2022), e09112, https://doi.org/10.1016/j.heliyon.2022.e09112.

[45] X. Chen, S.S. Mao, Titanium dioxide nanomaterials: synthesis, properties, modifications, and applications, Chem. Rev. 107 (7) (2007) 2891–2959, https://doi.org/10.1021/cr0500535.

[46] Z. Zhu, S. Wu, Y. Long, L. Zhang, X. Xue, Y. Yin, B. Xu, Phase-transition kinetics of silicon-doped titanium dioxide based on high-temperature X-ray-diffraction measurements, J. Solid State Chem. 303 (2021), 122544, https://doi.org/10.1016/j.jssc.2021.122544.

[47] C. Piffet, B. Vertruyen, F. Hatert, R. Cloots, F. Boschini, A. Mahmoud, High temperature X-ray diffraction study of the formation of $Na_2Ti_3O_7$ from a mixture of sodium carbonate and titaniumoxide, J. Energy Chem. 65 (2022) 210–218, https://doi.org/10.1016/j.jechem.2021.05.050.

[48] P.G. Callahan, J.-C. Stinville, E.R. Yao, Mc L.P. Echlin, M.S. Titus, M. De Graef, D.S. Gianola, T.M. Pollock, Transmission scanning electron microscopy: defect observations and image simulations, Ultramicroscopy 186 (2018) 49–61, https://doi.org/10.1016/j.ultramic.2017.11.004.

[49] J. Madejová, FTIR techniques in clay mineralstudies, Vib. Spectrosc. 31 (1) (2003) 1–10, https://doi.org/10.1016/S0924-2031(02)00065-6.

[50] M. Abdennouri, M. Baâlala, A. Galadi, M. El Makhfouk, M. Bensitel, K. Nohair, M. Sadiq, A. Boussaoud, N. Barka, Photocatalytic degradation of pesticides by titanium dioxide and titanium pillared purified clays, Arab. J. Chem. 9 (2016) S313–S318, https://doi.org/10.1016/j.arabjc.2011.04.005.

[51] V.J. González, E. Vázquez, B. Villajos, A. Tolosana-Moranchel, C. Duran-Valle, M. Faraldos, A. Bahamonde, Eco-friendly mechanochemical synthesis of titania-graphene nanocomposites for pesticide photodegradation, Separ. Purif. Technol. 289 (2022), 120638, https://doi.org/10.1016/j.seppur.2022.120638.

[52] L. Youssef, S. Roualdès, J. Bassil, M. Zakhour, V.R. Rouessac, C. Lamy, M. Nakhl, Effect of plasma power on the semiconducting behavior of low-frequency PECVD TiO_2 and nitrogen-doped TiO_2 anodicthin coatings: photo-electrochemical studies in a single compartment cell for hydrogen generation by solar water splitting, J. Appl. Electrochem. 49 (2019) 1–16, https://doi.org/10.1007/s10800-018-1265-4.

[53] M. Pawar, S. TopcuSendoğdular, P. Gouma, A brief overview of TiO_2 photocatalyst for organic dye remediation: case study of reaction mechanisms involved in Ce-TiO_2 photocatalysts system, J. Nanomater. 2018 (2018) e5953609, https://doi.org/10.1155/2018/5953609.

[54] P.C. Motsaathebe, O.E. Fayemi, Electrochemical detection of ascorbic acid in oranges at MWCNT-AONP nanocomposite fabricated electrode, Nanomaterials 12 (4) (2022) 645, https://doi.org/10.3390/nano12040645.

[55] Y. Wu, P. Deng, Y. Tian, J. Feng, J. Xiao, J. Li, J. Liu, G. Li, Q. He, Simultaneous and sensitive determination of ascorbic acid, dopamine and uric acid via an electrochemical sensor based on PVP-graphene composite, J. Nanobiotechnol. 18 (2020) 112, https://doi.org/10.1186/s12951-020-00672-9.

[56] G. Uwaya, O.E. Fayemi, Electrochemical detection of ascorbic acid in orange on Iron(III) oxide nanoparticles modified screen printed carbon electrode, J. Cluster Sci. (2021), https://doi.org/10.1007/s10876-021-02030-7.

[57] M. Choukairi, D. Bouchta, L. Bounab, Electrochemicaldetection of Uric Acid and Ascorbic Acid: Application in Serum, 2015, https://doi.org/10.1016/J.JELECHEM.2015.10.012.

[58] X. Zhang, Y.-C. Zhang, L.-X. Ma, One-pot facile fabrication of graphene-zinc oxide composite and its enhanced sensitivity for simultaneous electrochemical detection of ascorbic acid, dopamine and uric acid, Sensors and Actuators B-chemical 227 (2016) 488–496, https://doi.org/10.1016/J.SNB.2015.12.073.

[59] C. Karunakaran, S. Senthilvelan, Photooxidation of aniline on alumina with sunlight and artificial UV light, Catal. Commun. 6 (2) (2005) 159–165, https://doi.org/10.1016/j.catcom.2004.11.014.